Characterization of polymer surface structure and surface mechanical behaviour by sum frequency generation surface vibrational spectroscopy and atomic force microscopy

2004 J. Phys.: Condens. Matter 16 R659

(http://iopscience.iop.org/0953-8984/16/21/R02)

INSTITUTE OF PHYSICS PUBLISHING JOURNAL OF PHYSICS: CONDENSED MATTER

J. Phys.: Condens. Matter **16** (2004) R659–R677 PII: S0953-8984(04)59532-2

TOPICAL REVIEW

Characterization of polymer surface structure and surface mechanical behaviour by sum frequency generation surface vibrational spectroscopy and atomic force microscopy

Aric Opdahl[1], **Telly S Koffas**[1], **Ella Amitay-Sadovsky**[1,2], **Joonyeong Kim**[1] **and Gabor A Somorjai**[1,3]

[1] Department of Chemistry, University of California, Berkeley and Materials Sciences Division, Lawrence Berkeley National Laboratory, Berkeley, CA 94720, USA
[2] Department of Mechanical Engineering, University of California, Berkeley, CA 94720, USA

E-mail: somorjai@socrates.berkeley.edu

Received 23 September 2003, in final form 26 March 2004
Published 14 May 2004
Online at stacks.iop.org/JPhysCM/16/R659
DOI: 10.1088/0953-8984/16/21/R02

Abstract

Sum frequency generation (SFG) vibrational spectroscopy and atomic force microscopy (AFM) have been used to study polymer surface structure and surface mechanical behaviour, specifically to study the relationships between the surface properties of polymers and their bulk compositions and the environment to which the polymer is exposed. The combination of SFG surface vibrational spectroscopy and AFM has been used to study surface segregation behaviour of polyolefin blends at the polymer/air and polymer/solid interfaces. SFG surface vibrational spectroscopy and AFM experiments have also been performed to characterize the properties of polymer/liquid and polymer/polymer interfaces, focusing on hydrogel materials. A method was developed to study the surface properties of hydrogel contact lens materials at various hydration conditions. Finally, the effect of mechanical stretching on the surface composition and surface mechanical behaviour of phase-separated polyurethanes, used in biomedical implant devices, has been studied by both SFG surface vibrational spectroscopy and AFM.

(Some figures in this article are in colour only in the electronic version)

[3] Author to whom any correspondence should be addressed.

Contents

1. Introduction

The study of polymer surfaces and thin films includes synthetic, surface and colloid chemistry, as well as traditional materials and biomaterials science. Many industries depend on the surface properties of polymers in products involving coatings [1], colloidal stability [2, 3], lubrication and adhesion [4, 5], and biocompatibility [6]. Recent technological advances, for example, have seen polymer surfaces designed for use as biological scaffolds [7] and drug delivery systems [8], and also as nanopatterned templates and films for use in microelectronics [9], catalysis [10, 11] and sensor development [12]. The versatility of polymer films have made them ubiquitous in technological applications at smaller and smaller length scales. In order to understand the interaction of a polymer with its environment at these size regimes, it becomes increasingly important to have experimental measurements of the surface chemical and surface mechanical properties of these materials and to understand how these properties are modified as the environment is changed.

This review summarizes the results of three sets of experiments aimed at understanding polymer interface behaviour, using sum frequency generation (SFG) vibrational spectroscopy and atomic force microscopy (AFM). This combination of experimental techniques provides unique and complementary surface structure and surface mechanical behaviour information. SFG surface vibrational spectroscopy is an optical technique that is highly sensitive to the chemical composition, orientation and ordering of molecular groups at an interface. AFM can be used to map out the surface morphology and to probe the mechanical properties of the surface. Experiments can be designed, using each technique, to probe polymer/air and polymer/liquid interfaces, making this a powerful combination of tools for *in situ* studies. The first set of experiments are aimed at better understanding the surface segregation and wetting behaviour of polyolefin blends, used in car bumpers and other high-impact applications. In the second, the hydration dependence of the surface structure and mechanical properties of

hydrogel contact lens materials is presented. Finally, we present results showing the effect of mechanical stretching on the surface compositions and surface mechanical behaviours of phase-separated polyurethanes, used in biomedical implant devices.

2. Experimental methods and materials

2.1. SFG surface vibrational spectroscopy

Excellent descriptions of vibrationally resonant SFG have been presented in publications by Shen [13–16] and by Hirose [17]. The application of SFG surface vibrational spectroscopy to the study of polymer interfaces has recently been reviewed by Chen [18]. In our experiments, SFG vibrational spectra of polymer/air and polymer/liquid interfaces were obtained by overlapping two laser beams at the interface and measuring the light generated from the interface at the sum frequency. Vibrational spectra are generated when one of the beams is an infrared beam that is tuned over a region of interest. The picosecond laser and OPG/OPA system we have used to generate the visible beam (ω_1, 532 nm) and the tunable infrared beam (ω_2, 2000–4000 cm^{-1}) has been described elsewhere [19].

The intensity of the sum frequency signal, $I(\omega_s)$, is proportional to the square of the nonlinear susceptibility of the material, $\overleftrightarrow{\chi}^{(2)}$, a 27-component tensor (equation (1)). Under the electric-dipole approximation, all 27 components of $\overleftrightarrow{\chi}^{(2)}$ are equal to zero for centrosymmetric materials. Thus, materials that exhibit inversion symmetry, or that are randomly oriented in the bulk, are not expected to generate large sum frequency signals. However, if a material adopts a preferred anisotropic orientation at an interface, then symmetry is broken in the interface plane, and some of the components of $\overleftrightarrow{\chi}^{(2)}$ may be non-zero. Measurement of $\overleftrightarrow{\chi}^{(2)}$ is specifically sensitive to this type of ordering at an interface.

$$I(\omega_s) \propto |\chi^{(2)}|^2 \tag{1}$$

$$\overleftrightarrow{\chi}^{(2)} = \overleftrightarrow{\chi}^{(2)}_{NR} + n_s\left\langle\overleftrightarrow{\alpha}^{(2)}_{R}\right\rangle_f = \overleftrightarrow{\chi}^{(2)}_{NR} + \sum_q \frac{\overleftrightarrow{A}_q}{\omega_2 - \omega_q + i\Gamma_q} \tag{2}$$

$$\overleftrightarrow{A}_q = n_s\left\langle\overleftrightarrow{a}_q\right\rangle_f.$$

The vibrationally resonant contribution to the nonlinear susceptibility, $\overleftrightarrow{\chi}^{(2)} = n_s\langle\overleftrightarrow{\alpha}^{(2)}_{R}\rangle_f$, is enhanced when the infrared beam (ω_2) is tuned near a vibrational mode belonging to one of the molecular groups at the interface (ω_q). The term $\alpha^{(2)}$ is the molecular hyperpolarizability and can be related to the product of the dynamic dipole and polarizabilities of a vibrational mode. Thus, the mode must be both IR- and Raman-active in order to be measured. In equation (2), $\overleftrightarrow{A}_q$ is the strength and Γ_q is the damping term associated with the qth vibrational mode. The measured $\overleftrightarrow{A}_q$ for a particular vibrational mode depends on the number density of contributing molecular groups at the surface, n_s, and the orientation averaged nonlinear polarizability of those groups (brackets denote an average over a distribution function, f).

Surface vibrational spectra presented in this paper were obtained in the CH (2700–3100 cm^{-1}) stretching region using the $s_{sum}s_{vis}p_{IR}$ polarization combination and were fit using equations (1) and (2) in order to extract peak positions and amplitudes. If the components of $\overleftrightarrow{a}_q$ for a vibrational mode are known, then the measured $\overleftrightarrow{A}_q$ can be used to estimate the number density and orientation of the ordered molecular groups giving rise to the vibration in the interface region. Methods for estimating a_q for C–H vibrational modes are given in [14] and [17].

2.2. AFM

Topographic and friction images, as well as measurements of mechanical properties, were collected using a commercial AFM and a homebuilt, walking-style AFM. The homebuilt AFM is completely enclosed within a glass bell jar. Relative humidity (RH) can be varied by balancing the evaporation of water from a reservoir with a steady flow of nitrogen through the chamber. Decreasing the flow rate of nitrogen increases the experimental humidity, which is measured by a digital hydrometer placed within the chamber.

2.3. Polymers

Low and high molecular weight atactic polypropylene (*a*PP, $M_w \sim 50\,000$ and $\sim$200 000), aspecific polyethylene-*co*-propylene rubber (*a*EPR, $M_w \sim 50\,000$; 42 mol% ethylene randomly incorporated) and isotactic polypropylene (*i*PP, $M_w \sim 200\,000$) were synthesized by Basell Polyolefins, Inc. Further description of the physical properties of these polymers is available in [19] and [20]. Polystyrene was purchased from Scientific Polymer Inc. Further description of the poly(hydroxyethyl)methacrylate (pHEMA) hydrogels, provided by Ocular Sciences, Inc. are given in [21]. The polyurethane samples (copolymers of 42 and 69 wt% hard segments; hard segment, $M_w \sim 700$ and 1500 and soft segment $M_w = 1000$) were provided by the Polymer Technology Group and further description of their material properties can be found in [22].

3. Surface segregation in polyolefin copolymers and blends

This section summarizes SFG and AFM results obtained from the surfaces of polyolefins and polyolefin blends. The blend components include atactic polypropylene (*a*PP), isotactic polypropylene (*i*PP), and aspecific poly(ethylene-*co*-propylene rubber) (*a*EPR) [23, 20]. Blends of these materials serve as mimics for the important commercial blend of isospecific PP/EPR. A problem with PP/EPR blends is that they typically have poor adhesive properties—this is a characteristic of many crystalline polyolefins. The adhesive properties of the PP/EPR surface, however, have been observed to vary depending on the bulk composition and the processing conditions; therefore, it is important to understand how the surface composition is affected by both the blend composition and processing conditions.

Polymer/air interfaces of single-phase, bulk-miscible, polymer blends are usually enriched in the component which has the lowest surface energy. Most polymer blends are immiscible. The surface morphology of immiscible blends is complex, and complete wetting of the lower surface tension component is not always observed [24]. The combination of SFG vibrational spectroscopy and AFM is well suited for studying wetting phenomena. AFM experiments can distinguish blend components by differences in the mechanical properties of the polymer blend components and can be used to probe lateral phase separation at the interface, while SFG vibrational spectroscopy experiments can be used to determine the surface composition. This strategy was also used to characterize the surface composition of bulk-miscible biomedical polyurethane blends, and it was observed that the component with lowest surface tension migrated to the polymer/air interface [25].

3.1. Atactic polypropylene (aPP)/air and aspecific poly(ethylene-co-propylene) rubber (aEPR)/air interfaces

SFG spectra obtained from two of the individual blend components, *a*PP and *a*EPR, are shown in figure 1. In each of these spectra, the strongest feature is at 2883 cm^{-1} and is assigned as

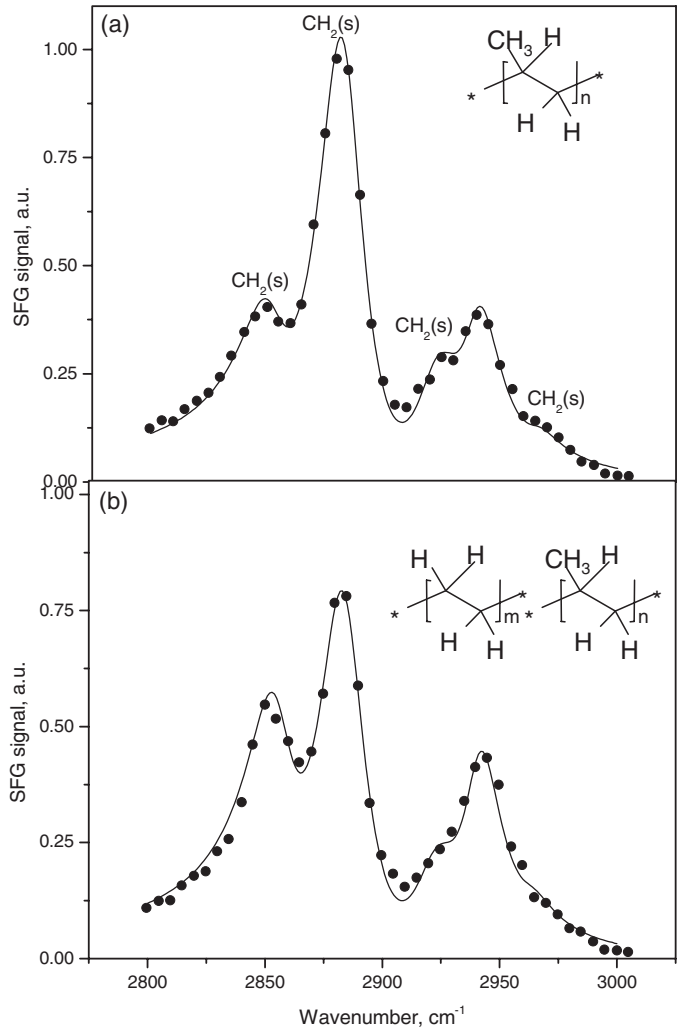

Figure 1. SFG spectra ($s_{\rm sum}s_{\rm vis}p_{\rm IR}$ polarization) of (a) atactic polypropylene (*a*PP)/air interface and (b) poly(ethylene-*co*-propylene) rubber (*a*EPR)/air interface.

the symmetric CH_3 stretch (CH_3(s)) from the methyl side branches [26, 19]. The feature at 2968 cm^{-1} is assigned to the asymmetric CH_3 stretch (CH_3(a)) from the side branch. Features at 2850 and 2920 cm^{-1} are assigned as the symmetric and asymmetric CH_2 stretches (CH_2(s) and CH_2(a)), respectively, from the polymer backbone. The feature at $\sim$2940 cm^{-1} is assigned as a Fermi resonance between the CH_3(s) stretch and an overtone of the CH_3 bending mode. In the following analysis, changes in intensity of the SFG signal from this Fermi resonance were not considered.

For CH_3 molecular groups, the peak associated with the CH_3(s) vibration will be strongest, and the ratio of the CH_3(s)/CH_3(a) peaks will be largest, in the ssp spectrum if the methyl groups are oriented upright. The large CH_3(s) peaks observed in figure 1 suggest that the methyl side branches have a tendency to preferentially order and order at the polymer/air interface for both *a*PP and *a*EPR. The ratio of the peaks associated with the CH_3(s)/CH_3(a)

is large and is similar for both polymers, indicating a similar upright orientation of the methyl side branches, for *a*PP and *a*EPR, at the interface. For the backbone CH_2 vibrations, the ratio of the $CH_2(s)/CH_2(a)$ peaks qualitatively contains the same type of orientation information as the methyl vibrations. Figure 1 shows that the SFG signal arising from the $CH_2(s)$ vibration (and the ratio of the $CH_2(s)/CH_2(s)$) is larger for *a*EPR as compared to *a*PP, which may be interpreted as a more upright interpretation of the CH_2 C_{2v} symmetry axis. However, analysis of the CH_2 vibrations in the 'ethylene-rich' *a*EPR copolymer is complicated by the fact that any adjacent CH_2 groups that are in a trans configuration will exhibit local inversion symmetry, and may not contribute to the measured SFG signal.

An important observation in the spectrum of *a*EPR is the small reduction in absolute intensity of the peak associated with the $CH_3(s)$ vibration, as compared to its intensity in the spectrum of *a*PP. The *a*EPR copolymer is comprised of ∼60% propylene monomers randomly incorporated in the polymer chain, and a given chain length has ∼60% as many methyl side branches as *a*PP. For this situation, the intensity of the peak associated with the $CH_3(s)$ vibration from *a*EPR should be ∼36% as intense (the A_q, should be 60% as large) as that from *a*PP. That the *a*EPR $CH_3(s)$ peak is enhanced in intensity suggests one of three possibilities:

(1) *a*EPR orders a higher percentage of methyl side branches at the surface compared to *a*PP,
(2) the methyl side branches are oriented more upright at the *a*EPR surface than they are at the *a*PP surface, or
(3) the methyl side branches are more tightly ordered for *a*EPR than they are for *a*PP.

A more detailed analysis of the A_q, extracted from the SFG spectra suggests that the most likely scenario is (1) and that the ethylene-rich *a*EPR copolymer orients a large excess of methyl branches at the interface compared to *a*PP [19].

This result from *a*PP and *a*EPR can be put into perspective with SFG results obtained from other relatively simple polymers. The SFG spectrum of polystyrene has been widely studied [27–30] and it has been observed that the phenyl side branches also preferentially order at this polymer/air interface. The situation is more complex for polymers with multiple side branches per monomer unit. For example, analysis of the SFG spectra of poly(hydroxyethyl)methacrylate (pHEMA) [21], which has a methyl side branch and a larger and more hydrophilic hydroxyethyl side branch suggests that the *smaller* low surface energy methyl branch preferentially orders at the polymer/air interface. In contrast, SFG results obtained from the surface of polymethylmethacrylate (PMMA) [31], which has a small methyl side branch and a much larger methyl methacrylate side branch, have shown that the dominant spectral feature is associated with the terminal methyl group in the larger ester side branch—indicating that the *larger* methyl ester side branch preferentially orients at the interface. Thus it appears that if the difference in surface tension of the competing side branches is large, then the side branch with lower surface tension will tend to order at the interface, while if the difference in surface tension is small, then the larger/bulkier side branch will tend to order at the interface.

3.2. aPP/aEPR blends

The surfaces of two amorphous blends of *a*PP/*a*EPR are compared in this section—a bulk miscible and a bulk immiscible blend. SFG spectra obtained from low molecular weight *a*PP (M_w 50 000), *a*EPR, and an annealed 50:50 wt% blend of the two components are shown in figure 2(a). Differential scanning calorimetry (DSC) results suggest that this blend is miscible in the bulk. Qualitatively, the SFG spectrum obtained from the blend surface is nearly identical to the spectrum obtained from the surface of *a*PP—indicating preferential segregation of *a*PP

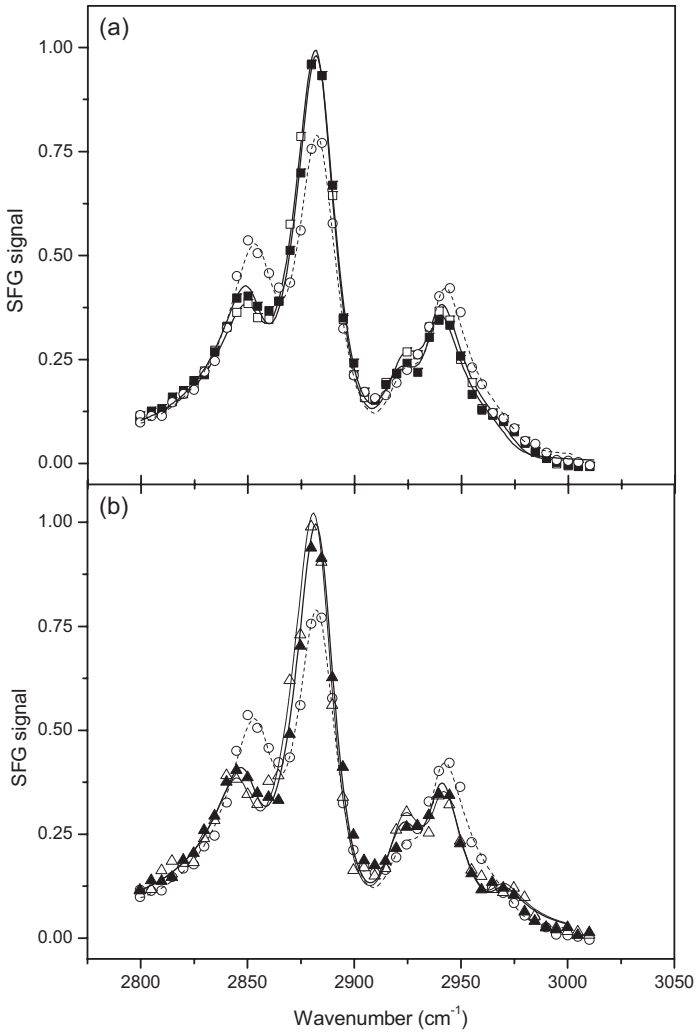

Figure 2. SFG spectra ($s_{\text{sum}}s_{\text{vis}}p_{\text{IR}}$ polarization) obtained from (a) low molecular weight *a*PP (open squares), *a*EPR (open circles), and a 50:50 bulk miscible *a*PP/*a*EPR blend (filled squares) after annealing and obtained from (b) high molecular weight *a*PP (open triangles), *a*EPR (open circle), and a 50:50 bulk immiscible *a*PP/*a*EPR blend (filled triangles) after annealing.

to the surface. Similar results were obtained from an *a*PP/*a*EPR blend where the molecular weight of the *a*PP component was increased from 50 000 to 200 000. DSC results show that this blend is immiscible in the bulk. In both the miscible and immiscible *a*PP/*a*EPR blends, SFG spectra (figure 2(b)) of an annealed film indicate that *a*PP segregates to the blend/air interface at the monolayer level.

In contrast, XPS spectra of the carbon valence band region can distinguish between the surface compositions of the bulk miscible and immiscible blends. XPS experiments have a surface sensitivity that is determined by the mean free path of photoelectrons generated in the polymer film, typically 2–10 nm, which is much deeper than the potential monolayer sensitivity of SFG experiments. XPS experiments were unable to detect surface enrichment of *a*PP in the bulk miscible *a*PP/*a*EPR blend. In connection with the SFG data, this suggests

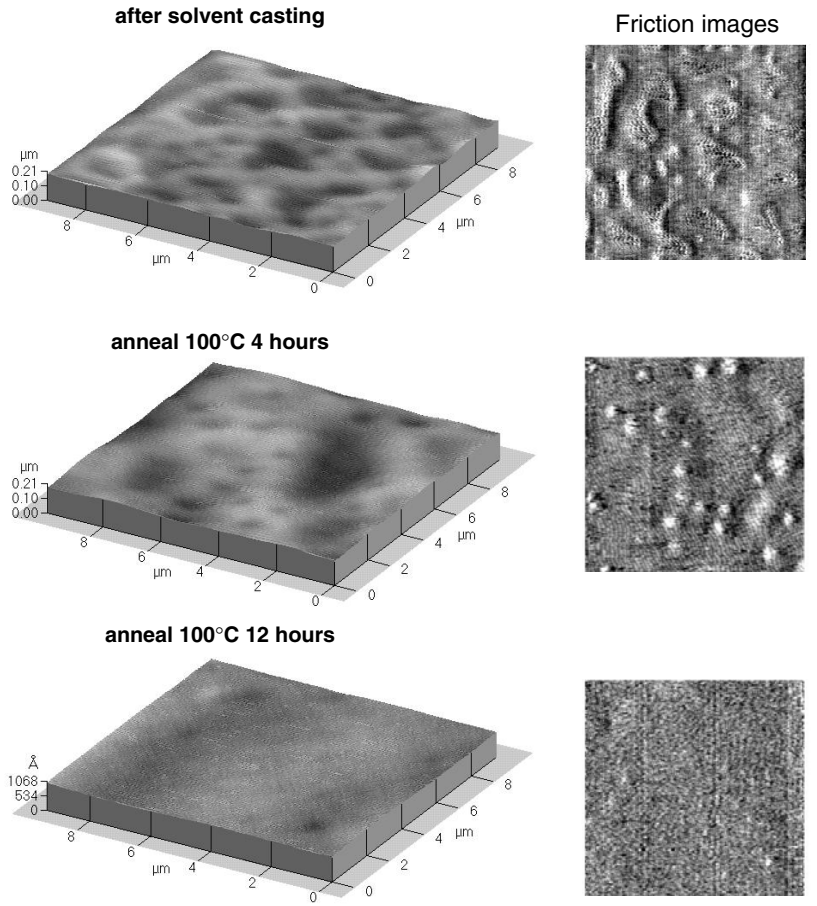

Figure 3. AFM topography and lateral force friction images of the bulk immiscible *a*PP/*a*EPR blend, showing polypropylene segregation as a function of annealing time. The dark regions in the topography image correspond to the bright regions in the lateral force image and are assigned as *a*EPR.

that the *a*PP surface enrichment layer in the miscible blend is very thin, and that the highest levels of *a*PP in the surface enrichment layer are restricted to the top 2–3 nm of the film. XPS spectra obtained from the bulk immiscible blend show significant enrichment of *a*PP in the surface region, suggesting that the *a*PP enrichment layer for the immiscible blend is thicker than 5–7 nm. Thus, for *a*PP/*a*EPR blends, we conclude that *a*PP wets the surface of the blend and that decreasing the miscibility increases the thickness of the surface enrichment layer.

AFM data support this conclusion. AFM images were used to monitor the wetting process in the *a*PP/*a*EPR blend. AFM images obtained from the miscible low molecular weight *a*PP/*a*EPR blends are homogeneous (amorphous) at all stages of annealing. SFG spectra [23] collected immediately after casting the blend contain CH_2 and CH_3 features that are intermediate in intensity to those of the two pure components, suggesting that 'as cast' *a*PP/*a*EPR blend surfaces may contain both components. Figure 3 shows AFM topography and lateral force images obtained from the surface of the bulk immiscible blend at various stages of the annealing process. Immediately after casting, the surface of the blend contains

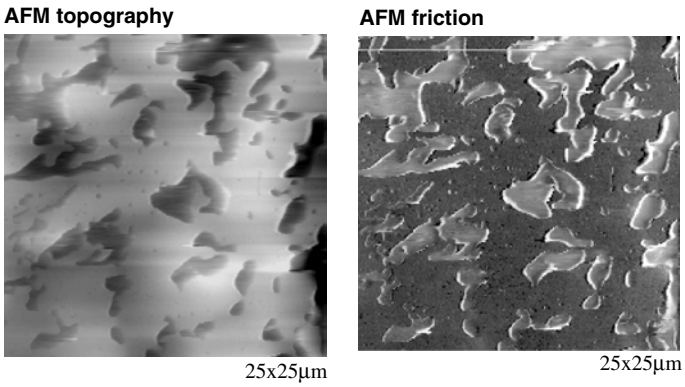

Figure 4. AFM topography and lateral force (friction) images of the *i*PP/*a*EPR blend melt pressed for 30 s. The dark (depressed) regions in the topography images correspond to the bright (high friction) regions in the lateral force image and are assigned as *a*EPR. The light regions in the topography images correspond to the dark regions in the lateral force image and are assigned as *i*PP.

two phases—the lateral force images show 'low friction' (dark) and 'high friction' (light) phases. As the blend is annealed, the AFM images show that the surface becomes smoother and that the 'high friction' regions become covered. Since the *a*EPR is much softer than the high molecular weight *a*PP component, the 'high friction' regions are assumed to be *a*EPR. This interpretation is consistent with the SFG data presented in figure 2 for the blend after annealing, and suggests that the *a*PP component wets the *a*EPR only after extended annealing periods.

3.3. iPP/aEPR blends

Crystallization can be used to trap surface morphologies in a nonequilibrium morphology. If isotactic polypropylene (*i*PP) is substituted for atactic polypropylene in the PP/*a*EPR blend, blend surfaces can be prepared that are enriched in *i*PP, enriched in *a*EPR, or that contain a phase-separated mix of the two components [20]. The isotactic component crystallizes when it cools from the melt and traps morphologies formed in the melt. Distinguishing between *i*PP and *a*EPR by AFM is straightforward as the *i*PP component is crystalline and the *a*EPR component is soft and amorphous. Figure 4 shows an AFM topography and corresponding friction image of the *i*PP/*a*EPR blend melt pressed between glass for 30 s and quenched to room temperature. The depressed regions (dark) in the topography image correspond to high friction (bright) regions in the friction image and have been assigned as *a*EPR. In this image, the depressions are an artifact caused by the tip pressing against the soft *a*EPR phase. For scans conducted at higher loads, the tip presses deeper into the surface of the blend.

When the blend is melt-pressed for longer times, the *i*PP and *a*EPR phases grow in size, but are both present at the surface after the pressing substrate is removed. When the blend is melted in open air, the surface appears crystalline by AFM. This suggests that *i*PP preferentially segregates to the air/polymer interface—consistent with the results obtained from the *a*PP/*a*EPR blends. For the *i*PP/*a*EPR samples, the surfaces of the air melt are too rough to obtain high-quality SFG spectra from them, however, XPS data and the AFM images suggest that the segregation layer of *i*PP is thick in this case.

After melt-pressing, the *a*EPR component can be enriched at the interface by exposing the blend to n-hexane solvent vapour. The *a*EPR component is soluble to n-hexane and the *i*PP

component is not. The solvent swells the *a*EPR and draws it to the interface. This is seen in AFM images obtained from *i*PP/*a*EPR surface, which appear amorphous and are mechanically softer after exposure to n-hexane vapour. The *a*EPR has better adhesive properties than the *i*PP component and drawing the *a*EPR component to the surface by solvent may improve the overall adhesive properties of the *i*PP/*a*EPR blend.

4. Surface molecular structure and surface mechanical properties of hydrogels, and adsorption at the polymer/liquid interface

Hydrogels have been used as soft contact lenses for vision correction for over 30 years. In spite of the many advances that have been made to improve the comfort and biocompatibility of contact lenses, the interfacial properties of contact lens hydrogels, including surface hydration, are not well understood [32]. It is generally believed that high water content and high surface hydrophilicity are desirable properties, in order to increase the wettability of tear films [33]. Surface water content is particularly important for poly(hydroxyethyl)methacrylate (pHEMA) based contact lenses, which tend to dehydrate and become glassy and rigid when they are on the eye [34]. Additionally, when a contact lens hydrogel is placed on the eye, protein material adsorbs to the lens from the tear fluid, which eventually leads to discomfort for the wearer.

AFM and SFG are a powerful combination of tools for studying the mechanical behaviour and composition of the hydrogel surface, as well as the adsorption of macromolecules to that surface. Both techniques are capable of measuring properties at the hydrogel/air and hydrogel/liquid interfaces [21, 35, 36]. SFG is capable of probing the molecular rearrangements that occur at buried polymer/liquid interfaces [37]. A schematic of the AFM sample holder used to study both types of interface is shown in figure 5(a). AFM measurements were made on fully hydrated hydrogels at the hydrogel/water interface, fully dehydrated (no saline in the reservoir) hydrogels at the hydrogel/air interface, and hydrogels exposed to controlled humidity air at the hydrogel/humidified air interface. SFG and AFM experiments were performed in a similar manner, but flat hydrogel samples were used for SFG experiments instead of curved contact lens hydrogels. The surfaces of two hydrogels were compared: (a) a neutral pHEMA hydrogel (38 wt% water when fully hydrated) and (b) an ionic hydrogel comprised of a copolymer of pHEMA and methacrylic acid (55 wt% water when fully hydrated).

5. Surface molecular structure of hydrogels and adsorption at the polymer/liquid interface

SFG spectra obtained from the hydrogel/water interface are observed to be featureless (figure 6(a)). This type of behaviour was also observed for polystyrene that was exposed to toluene (solvent) vapour [38]. Toluene is a solvent for polystyrene and will readily penetrate a polystyrene film at ambient temperature. SFG spectra obtained from the toluene liquid/vapour interface showing that in addition to coating the surface of polystyrene, toluene penetrates and disrupts the ordering of the underlying polystyrene film. The results for pHEMA suggest that, like the hydrophobic polystyrene/toluene interface, the water swollen hydrogel is not highly ordered at the hydrogel/water interface. SFG spectra obtained from dehydrated hydrogels at the air interface show contributions from the low surface energy methyl side branch [21] (figure 6(b)).

AFM indentation (force versus distance) curves collected from the surfaces of fully hydrated pHEMA and pHEMA + MA hydrogels are shown in figure 5(b). For reference, a force versus distance curve collected against a hydrophilic silica surface is also shown in

(a) AFM liquid cell

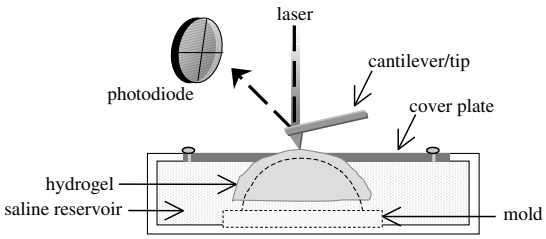

(b) AFM force-distance curves and associated hydrogel mechanical properties

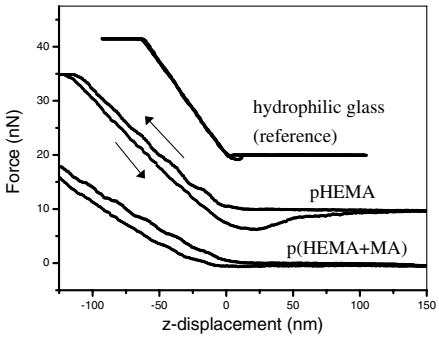

	Elastic modulus (MPa)	Adhesion (nN)	Friction coeff. (mV/nN)
pHEMA lens (water=38%)	1.34 ± 0.13	3.7 ± 0.4	12.3 ± 0.4
pHEMA+MA lens (water=55%)	0.47 ± 0.04	~0	1.45 ± 0.05

Figure 5. (a) Schematic of the hydrogel sample holder used for AFM experiments. The hydrogel is supported on a polypropylene mold, placed in a reservoir containing saline solution, and then covered by a stainless steel plate with an aperture to allow the AFM tip to access the hydrogel/air or hydrogel/water interfaces. (b) AFM force versus distance indentation curves obtained from a reference hydrophilic silica surface, fully hydrated pHEMA lens in water, and fully hydrated ionic pHEMA + MA hydrogel in water using a polystyrene AFM tip. A table showing the mechanical properties extracted from the force–distance curves is provided to the right.

figure 5(b). These indentation curves measure the bending of the AFM cantilever as the AFM tip presses against the hydrogel surface and is then retracted from the hydrogel. The slopes of the approach and retract curves contain information related to the stiffness, elastic modulus and viscoelastic relaxation of the hydrogel surface.

A large (1 μm radius of curvature) polystyrene AFM tip was used to produce the indentation curves shown in figure 5(b). This tip applies lower pressure to the hydrogel than a conventional 20 nm radius of curvature tip. The slope of the pHEMA + MA curve is smaller than the slope of the pHEMA curve. The lower slope obtained from the pHEMA + MA surface suggests a lower stiffness and elastic modulus for the pHEMA + MA hydrogel surface—consistent with the lower bulk modulus of this higher water content hydrogel. Estimates of the elastic modulus are consistent with the measured bulk values. The adhesion (pull-off force) measured between the polystyrene AFM tip and the hydrogel surface is higher for the neutral pHEMA hydrogel than it is for the ionic pHEMA + MA lens. In aqueous solution, this type of hydrophobic interaction leads to large adhesion values [39].

To further understand this type of phenomenon, we have used SFG to investigate the molecular structure and ordering of amphiphilic neutral polymers, polypropylene glycol (PPG), polyethylene glycol (PEG) and a triblock PEG–PPG–PEG copolymer (structures are shown in figure 7(b)), adsorbed on hydrophobic polystyrene and hydrophilic silica surfaces at the solid/liquid interface [40]. In the case of adsorption of macromolecules to hydrophobic surfaces

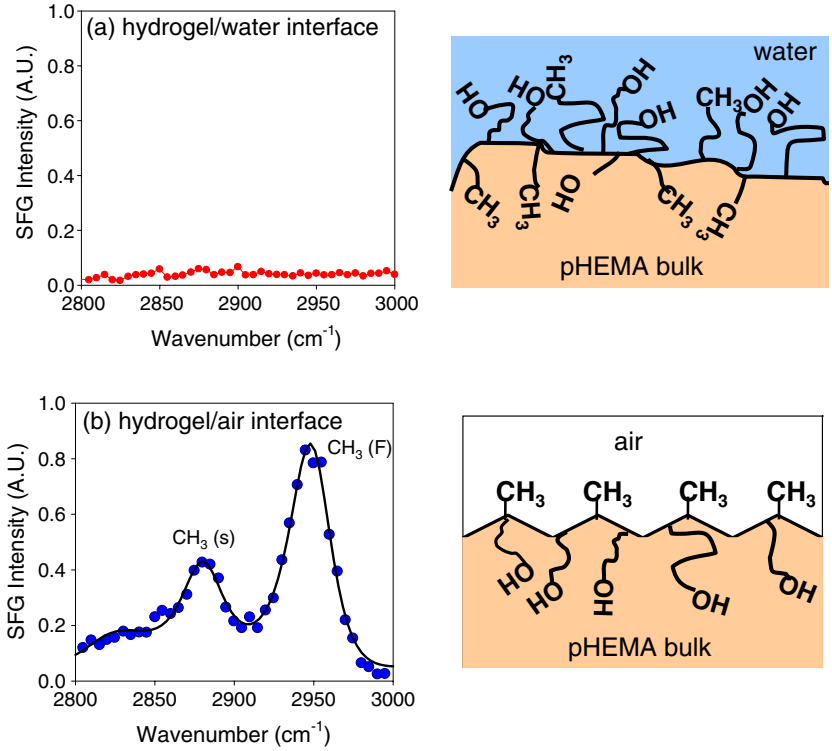

Figure 6. SFG spectra ($s_{\rm sum}s_{\rm vis}p_{\rm IR}$ polarization) of the (a) hydrogel/water and (b) hydrogel/air interfaces. No SFG signal is obtained at the water interface, suggesting that the hydrogel surface is disordered. At the air interface, the lower surface energy methyl side branch is found to order.

in aqueous solution, the driving force for the interaction is the entropy change associated with the removal of ordered water from the hydration shell of the macromolecules and the substrate into the aqueous bulk phase [41–44]. In addition to aiding the understanding of the high adhesion measured between polystyrene and pHEMA, these types of experiment are important for understanding the basic mechanisms of adsorption and denaturation of proteins at interfaces [45].

SFG spectra in the CH-stretch region obtained from amphiphilic neutral PPG, PEG and a PEG–PPG–PEG copolymer adsorbed on hydrophobic polystyrene and hydrophilic silica substrates from aqueous solution are shown in figures 7(a) and (b), respectively. In order to separate the contributions to the SFG signal from the adsorbed polymers and underlying polystyrene, perdeuterated polystyrene was used.

When adsorbed on hydrophobic polystyrene surfaces, the SFG spectrum for PPG contains features around 2840, 2870, 2940 and 2970 $\rm cm^{-1}$, assigned to the CH_2(s), CH_3(s), CH_3 Fermi resonance (CH_3(F)), and CH_3(a) modes, respectively (figure 7(a)) [46]. Figure 7(a) also shows the SFG spectrum of PEG absorbed on polystyrene from aqueous solution. PEG is more hydrophilic and has a higher solubility in water compared to PPG. This spectrum contains vibrational features around 2865 and 2935 $\rm cm^{-1}$, corresponding to the CH_2(s) and CH_2 Fermi resonance (CH_2(F)) modes, respectively [47]. These two SFG spectra suggest that adsorbed PPG and PEG molecules order at the hydrophobic polystyrene/water interface. The SFG spectrum for a triblock copolymer (PEG–PPG–PEG) adsorbed on hydrophobic polystyrene

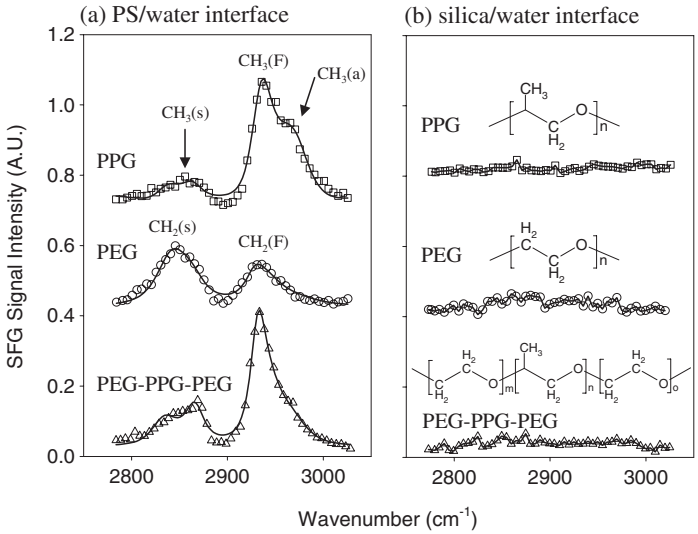

Figure 7. SFG spectra ($s_{sum}s_{vis}p_{IR}$ polarization) for adsorbed PPG (□), PEG (◯) and PEG–PPG–PEG (△) at (a) the hydrophobic perdeuterated polystyrene (PS)/water and (b) hydrophilic silica/water interfaces. The structures of PPG, PEG and a triblock PEG–PPG–PEG copolymer are also shown.

surfaces contains features similar to the spectrum obtained from PPG. This suggests that the more hydrophobic PPG centre block orders, producing an SFG signal, whereas the more hydrophilic PEG end blocks are disordered when the triblock copolymer adsorbs on the hydrophobic polystyrene.

To test the role that the hydrophobic solid surface plays in amphiphilic neutral polymer ordering, a similar set of experiments was conducted using bare silica substrates in place of polystyrene. Clean silica surfaces are generally regarded as hydrophilic because of the presence of surface silanol groups (Si–OH) and can be prepared as described elsewhere [48]. SFG spectra in figure 7(b) show no spectral features for any of the polymers adsorbed at the silica/water interface, despite large amounts of polymer adsorption. This indicates that when amphiphilic neutral polymers like PPG, PEG and PEG–PPG–PEG adsorb on hydrophilic surfaces, they do not preferentially orient their hydrophobic or hydrophilic moieties [49].

Water is also necessary to mediate the alignment of adsorbed polymers at the solid/liquid interface. To demonstrate the role of water in the alignment of adsorbed polymers at the interface, a set of experiments was performed using deuterated methanol in place of water as a solvent. SFG spectra obtained from the hydrophobic polystyrene surfaces and hydrophilic silica surfaces in contact with PPG/methanol solutions contained no measurable features, indicating that polymers adsorbing on the substrates do not display ordering [50]. Similar results were obtained for PEG and the triblock PEG–PPG–PEG copolymer.

SFG results indicate that hydrophobic surfaces along with water as a solvent are required for the ordering of adsorbed amphiphilic neutral polymers. Our SFG studies have revealed that PPG, PEG and a triblock PEG–PPG–PEG copolymer preferentially order when they adsorb at the hydrophobic polystyrene/water interface. These polymers disorder at hydrophilic silica/water and hydrophobic polystyrene/methanol interfaces. From this series of experiments, it is likely that the ordering of adsorbed amphiphilic neutral polymers depends on surface hydrophobicity and solvent via hydrophobic interactions.

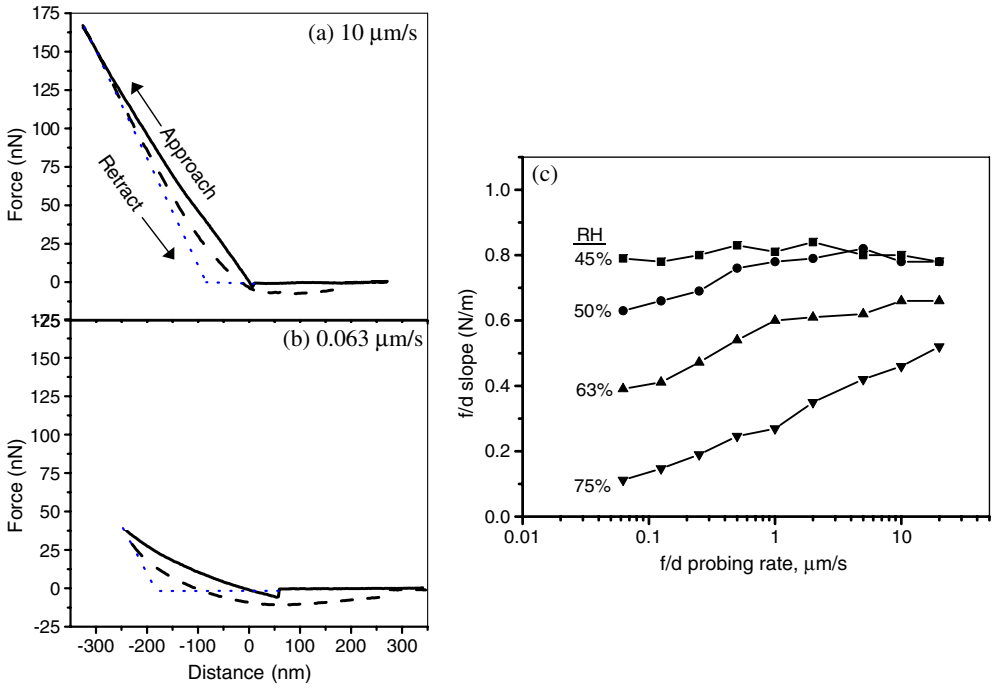

Figure 8. AFM force versus distance indentation curves obtained from a pHEMA hydrogel exposed to 75% relative humidity. Indentation curve (a) was collected at 10 μm s^{-1} and curve (b) was collected at 0.063 μm s^{-1}. (c) Rate dependence of the indentation curve slope for various humidity values.

This may indicate that part of the high adhesion between pHEMA and polystyrene correlates to ordering of pHEMA methyl side branches at the pHEMA/polystyrene interface. Charged polymers do not show ordering at polystyrene. For the ionic hydrogel pHEMA + MA, the lower adhesion between the hydrogel and the tip is associated with the lower friction coefficient measured for the pHEMA + MA hydrogel compared to the pHEMA hydrogel surface.

5.1. Humidity dependence of mechanical properties

AFM force versus distance curves can be obtained at various rates. The measurement of rate-dependent surface mechanics provides information concerning the viscoelastic properties and relative hydration of the hydrogel surface at different humidities. Figures 8(a) and (b) show two AFM indentation curves obtained at different probing rates from the surface of a bulk hydrated pHEMA hydrogel at 75% relative humidity, using a sharper (20 nm radius of curvature) silicon nitride AFM tip [35]. For the curve obtained at a slower probing rate, the cantilever bends less (the slope of the approach curve is smaller), indicating that for slower loading rates the AFM tip can press more deeply into the hydrogel as the polymer chains relax. Relaxation of the pHEMA hydrogel surface can be qualitatively assessed by measuring the slope of the approach curve as a function of probing rate. Figure 8(c) shows the dependence of the approach curve slope on the probing rate for humidity values between 45% and 80%.

At low humidity, there is little rate dependence in the indentation curves. The slopes of the indenting (approach) curves measured from bulk-hydrated hydrogels at low humidity are sim-

ilar to those measured from bulk-dehydrated hydrogels. Bulk-dehydrated pHEMA hydrogels are glassy. This indicates that at low humidity, the hydrogel/air interface region of the bulk-hydrated hydrogel is dry. At higher humidity values, the rate dependence of the indentation curves becomes more pronounced. At higher humidity the surface region of the bulk-hydrated lens contains more water as the rate of dehydration from the surface decreases. Under saturated humidity conditions, SFG spectra obtained from the air-exposed surface of bulk-hydrated pHEMA show contributions from the hydroxyethyl side branch, which were not observed for the dehydrated sample. The presence of an SFG signal, however, suggests that at the monolayer level, the pHEMA surface is not fully hydrated, even under saturated humidity conditions.

Similar data was obtained from the surface of pHEMA + MA [36]. The surfaces of both pHEMA and pHEMA + MA hydrogels are dry and glassy at low humidity and become soft as the humidity increases. However, the surface of pHEMA + MA requires a longer timescale to dissipate stress during loading than does the pHEMA + MA lens, at a given humidity value. At a given humidity, the pHEMA lens surface is softer and retains more water than the pHEMA + MA lens, even though the bulk contains less water. This suggests that the neutral hydrogel contains more strongly bound water at the surface than the ionic hydrogel. This observation correlates with clinical trials suggesting that ionic hydrogels tend to dehydrate faster on the eye than neutral hydrogels.

In summary, AFM is a powerful method to measure changes in the mechanical properties of hydrogels. The differences in the onset of viscoelastic behaviour, as well as differences in surface stiffness and work of adhesion between pHEMA and p(HEMA+MA) point to lower interfacial water content for p(HEMA+MA). Prior clinical and experimental observations also show interfacial water content is compromised in high bulk water content lenses. As the humidity is increased, pHEMA chains at the surface reorient to allow their hydrophilic hydroxyethyl groups to replace pendant methyl groups. The presence of an SFG signal suggests that the pHEMA surface is never fully hydrated, even under saturated humidity conditions.

6. Structure and surface mechanical behaviour of stretched polyurethanes

The mechanical environment can also affect polymer surface morphology. Most polymers can be deformed/stretched to some extent. Stretching has the effect of increasing the surface to volume ratio of a polymer. Macroscopically, the dimensions of an initially flat polymer surface change as a result of stretching—the surface becomes longer and thinner. For multi-component polymers, changes in surface area/shape can potentially lead to changes in the surface composition, based on differences in mechanical properties of the individual components. The deformation of polymers by stretching is important in industry and in biological systems, such as skin and heart tissue. Thus, the effects of stretching on polymer surface structure, composition and mechanical properties are significant, as it is the polymer interface that interacts with the environment when the polymer is deformed.

Elastomers usually have a rubbery, flexible phase that absorbs strain energy (at low elongation) and a crystalline (or rigid) phase. Polyurethane (PUR) copolymers are widely used as biomedical implants due to their superior mechanical properties and good biocompatibility [51–54]. PUR copolymers exhibit a two-phase structure consisting of immiscible short soft and hard segments (710–1450 g mol^{-1}). The large number of hydrogen bonding sites in the urethane groups results in strong interactions between the hard segments, leading to the formation of ordered hydrogen-bonded nanodomains [55]. The stretching mechanisms of PUR block copolymers were studied by AFM and SFG. AFM was used to obtain nanomechanical and topographical measurements and SFG vibrational spectroscopy was used to study changes in the conformation of the polyurethane backbone at the polymer/air

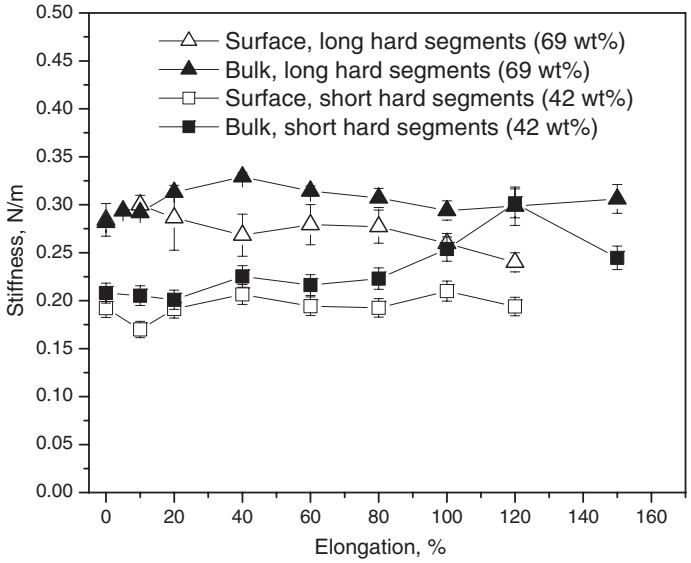

Figure 9. Surface stiffness and bulk stiffness as a function of elongation for 42% and 69% hard segment polyurethanes. Surface stiffness was derived from AFM indentation curves. For both copolymer compositions, the surface is stiffer than the bulk.

interface as the PUR was elongated. Details of the stretching device and the experimental setup are given elsewhere [22, 56].

Figure 9 shows the effects of elongation on the surface stiffness for two indentation depth regions and for two different PUR compositions. Stiffness was obtained from AFM indentation curves. Each stiffness value obtained for indentation depths of the order of ∼115 nm will be referred to as a *bulk* stiffness, while a stiffness value extracted from nanoindentation measurements obtained for depths less than ∼15 nm will be referred to as a *surface* property. The two PUR copolymers contain 42% and 69% hard segments, respectively. The copolymer with 69% hard segments has longer hard segments than the copolymer with 42% hard segments.

Figure 9 shows that prior to elongation, the copolymer with 69% hard segments has a larger surface stiffness than the copolymer with 42% hard segments. The PUR copolymer with 69% hard segments has lower surface adhesion and roughness compared to PUR films with 42% hard segments [22]. The effect of stretching on the surface stiffness is secondary. Figure 9 shows that, for the 69% hard segment PUR compositions, the surface and bulk stiffness are similar at elongations smaller than 10%. However, for elongations greater than 10%, the surface stiffness of the 69% hard segment copolymer is consistently lower than the bulk stiffness. The different mechanical responses of the surface and bulk regions may be attributed to microstructural changes (i.e. differences in the packing of the molecular chains in these regions).

SFG spectra of the 42% and 69% hard segment PUR copolymers are shown in figures 10(a) and (d), respectively. Qualitatively, both spectra are similar to the SFG spectrum obtained from the pure soft segment (polytetramethyloxide, PTMO) [56]. The ratio of the peak intensities of the PUR with long hard segments is somewhat different than that of PTMO and a detailed analysis of these differences is given elsewhere [56]. This general similarity suggests that the surface composition of the as-cast PUR films is enriched with soft segments. This is supported by the lower surface tension of the soft segment compared to that of the hard segment, the

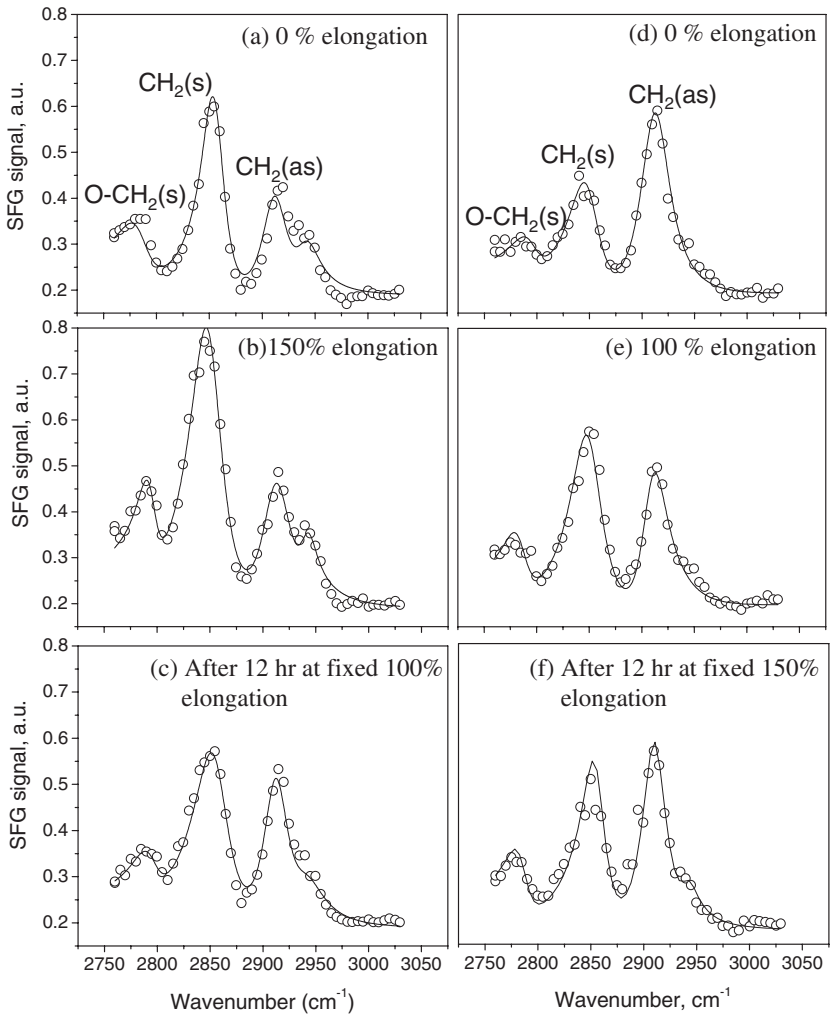

Figure 10. SFG spectra ($s_{sum}s_{vis}p_{IR}$ polarization) of 42% hard segment polyurethanes (a) prior to elongation, (b) immediately after elongating to 150% and (c) after holding the polymer at 150% elongation for 12 h. SFG spectra of 69% hard segment polyurethanes (d) prior to elongation, (e) immediately after elongating to 100% and (f) after holding the polymer at 100% elongation for 12 h.

AFM indentation results showing that the surface is less stiff (softer) than the bulk material, and complementary XPS data suggesting a depletion of hard segments in the near surface region.

Figure 10 also shows SFG spectra obtained from the PUR films containing 42% (figure 10(b)) and 69% (figure 10(e)) hard segments at 150 and 100% elongations, respectively. Elongation changes the spectra of both copolymers. For both PUR compositions, the CH_2(s) peak intensifies with elongation compared to the CH_2(a) peak, resulting in CH_2(s)/CH_2(a) ratios of PUR with 42% and 69% hard segments that are higher than the corresponding values of the as-cast compositions. The larger ratio suggests that the backbone CH_2 segments contributing to the SFG signal orient in a more upright direction as the polymers are elongated. Stretching a polymer chain is expected to promote ordering of the backbone in the direction of the stretch. Additionally, the peak associated with the soft segment (2795 cm^{-1}) decreases in intensity relative to the other peaks in the spectrum, suggesting enrichment of hard segments (or

depletion of soft segments) at the surface. Under stretching, the soft segments elongate at the surface, exposing the underlying hard segments at the surface. This mechanism also explains the increase in stiffness and reduction in adhesion of PUR with longer/higher percentage of hard segments.

Although the $CH_2(s)/CH_2(a)$ mode strength ratio increases when the polymers are initially elongated, maintaining the films at a constant elongation for 1 and 12 h decreases the mode strength ratio for both film compositions as the polymer surface restructures. This is most noticeable for PUR with 42% hard segments. This relaxation process was observed for a relatively long time (i.e. 1–12 h) and resulted in irreversible changes in the structure and chemical composition of the polymer surface. Interestingly, after repeated stretching and relaxation, the spectra obtained from both copolymer compositions (42% and 69%) appear similar (figures 10(c) and (f)). This shows that when polymers are subjected to repeated stress, their surface chemistry can change. Thus, if a polymer is to be used in this type of situation (as in a heart valve), in addition to designing the surface chemistry (specific surface functional groups), the material should be designed such that the surface chemical composition is resistant to change when it is subjected to mechanical stress.

In summary, this study has shown that the alternation of the surface chemical composition due to stretching can be tracked by using the surface vibrational spectrum of each polyurethane component as a fingerprint. By correlating the chemical data to the surface elasticity determined from nanoindentation experiments, a better understanding of the mechanical properties, structure and composition of the polymer surface during stretch can be acquired. The results suggest that under stretching, the soft segments elongate at the surface, thus occupying a lower percentage of the surface. This mechanism also explains the increase in stiffness and reduction in adhesion of PUR with a higher percentage of hard segments.

7. Conclusions

When information obtained from AFM is combined with that obtained from molecular structure information obtained from SFG surface spectroscopy, a more detailed understanding of events occurring at interfaces is obtained. The combination of SFG and AFM was used to study the surface segregation and wetting behaviour of polyolefin blends. In that example, SFG experiments provided an average surface composition while AFM images were able to show the lateral structure of the surface. Both techniques were used to probe the surface structure and mechanical properties of hydrogel contact lens materials as a function of hydration. Finally, the effect of mechanical stretching on the surface composition and surface mechanical behaviour of phase-separated polyurethanes, used in biomedical implant devices, was studied by both techniques.

Acknowledgments

This work was supported by the Director, Office of Science, Office of Basic Energy Sciences, Division of Materials Sciences and Engineering, of the US Department of Energy under Contract No DE-AC03-76SF00098. The authors acknowledge support from Basell Polyolefins, Ocular Sciences Inc., and the Polymer Technology Group.

References

[1] Wicks Z W 1992 *Organic Coatings: Science and Technology* (New York: Wiley)
[2] Goodwin J W and Buscall R 1995 *Colloidal Polymer Particles* (London: Academic)
[3] Kawaguchi H 2000 *Prog. Polym. Sci.* **25** 1171
[4] Israelachvili J 1992 *J. Vac. Sci. Technol.* A **10** 2961
[5] Aoike T, Uehara H, Yamanobe T and Komoto T 2001 *Langmuir* **17** 2153

[6] Castner D G and Ratner B D 2002 *Surf. Sci.* **500** 28
[7] Karp J M, Dalton P D and Shoichet M S 2003 *Mater. Res. Soc. Bull.* **28** 301
[8] Davis K A and Anseth K S 2002 *Crit. Rev. Ther. Drug.* **19** 385
[9] Ito H, Tagawa S and Horie K (ed) 1994 *Polymeric Materials for Microelectronics Applications: Science and Technology* (Washington, DC: American Chemical Society)
[10] Wuff G 2002 *Chem. Rev.* **102** 1
[11] Kralik M and Biffis A 2001 *J. Mol. Catal.* A **177** 113
[12] Akmal N and Usmani A M (ed) 1998 *Polymers in Sensors: Theory and Practice* (Washington, DC: American Chemical Society)
[13] Shen Y R 1984 *Principles of Nonlinear Optics* (New York: Wiley)
[14] Wei X, Hong S C, Zhuang X W, Goto T and Shen Y R 2000 *Phys. Rev.* E **62** 5160
[15] Miranda P B and Shen Y R 1999 *J. Phys. Chem.* B **103** 3292
[16] Zhuang X, Miranda P B, Kim D and Shen Y R 1999 *Phys. Rev.* B **59** 12632
[17] Hirose C, Akamatsu N and Domen K 1992 *Appl. Spectrosc.* **46** 1051
[18] Chen Z, Shen Y R and Somorjai G A 2002 *Annu. Rev. Phys. Chem.* **53** 437
[19] Opdahl A, Phillips R A and Somorjai G A 2002 *J. Phys. Chem.* B **106** 5212
[20] Opdahl A, Phillips R A and Somorjai G A 2003 *J. Polym. Sci.* B at press
[21] Kim S H, Opdahl A, Marmo C and Somorjai G A 2002 *Biomaterials* **23** 1657
[22] Amitay-Sadovsky E, Ward B, Somorjai G A and Komvopoulos K 2002 *J. Appl. Phys.* **91** 375
[23] Opdahl A, Phillips R A and Somorjai G A 2002 *Macromolecules* **35** 4387
[24] Wang H and Composto R J 2002 *Macromolecules* **35** 2799
[25] Zhang D, Gracias D H, Ward R, Gauckler M, Tian Y, Shen Y R and Somorjai G A 1998 *J. Phys. Chem.* B **102** 6225
[26] Zhang D, Shen Y R and Somorjai G A 2002 *Chem. Phys. Lett.* **281** 394
[27] Zhang D, Dougal S M and Yeganeh M S 2000 *Langmuir* **16** 4528
[28] Gautam K S, Schwab A D, Dhinojwala A, Zhang D, Dougal S M and Yeganeh M S 2000 *Phys. Rev. Lett.* **85** 3854
[29] Briggman K A, Stephenson J C, Wallace W E and Richter L J 2001 *J. Phys. Chem.* B **105** 2785
[30] Oh-e M, Hong S C and Shen Y R 2002 *Appl. Phys. Lett.* **80** 784
[31] Wang J, Chen C, Buck S M and Chen Z 2001 *J. Phys. Chem.* B **105** 12118
[32] McConville P and Pope J M 2001 *Polymer* **42** 3559
[33] Lopez-Alemany A, Compan V and Refojo M F 2002 *J. Biomed. Mater. Res.* A **63** 319
[34] Pritchard N and Fonn D 1995 *Opthalmic Physiol. Opt.* **15** 281
[35] Opdahl A, Kim S H, Koffas T S, Marmo C and Somorjai G A 2003 *J. Biomed. Mater. Res.* A **67** 350
[36] Koffas T S, Opdahl A, Marmo C and Somorjai G A 2003 *Langmuir* **19** 3453
[37] Wang J, Paszti Z, Even M A and Chen Z 2002 *J. Am. Chem. Soc.* **124** 7016
[38] Opdahl A and Somorjai G A 2002 *Langmuir* **18** 9409
[39] Sinniah S K, Steel A B, Miller C J and Reutt-Robey J E 1996 *J. Am. Chem. Soc.* **118** 8925
[40] Kim J, Opdahl A, Chou K C and Somorjai G A 2003 *Langmuir* **19** 9551
[41] Tanford C 1991 *The Hydrophobic Effect: Formation of Micelles and Biological Membranes* 2nd edn (Malabar, FL: Krieger)
[42] Zhang X, Zhu Y and Granick S 2001 *J. Am. Chem. Soc.* **123** 6736
[43] Eisenberg D and McLachlan A D 1986 *Nature* **319** 199
[44] Muller N 1990 *Acc. Chem. Res.* **23** 23
[45] Horbett T A and Brash J L (ed) 1995 *Proteins at Interfaces II: Fundamentals and Applications* (Washington, DC: American Chemical Society)
[46] Fontyn M, van't Riet K and Bijsterbosch B H 1991 *Colloids Surf.* **54** 349
[47] Chen C, Even M A, Wang J and Chen Z 2002 *Macromolecules* **35** 9130
[48] Iler R K 1979 *The Chemistry of Silica* (New York: Wiley)
[49] Dreesen L, Humbert C, Hollander P, Mani A A, Ataka K, Thiry P A and Peremans A 2001 *Chem. Phys. Lett.* **333** 327
[50] Stanners C D, Du Q, Chin R P, Cremer P, Somorjai G A and Shen Y R 1995 *Chem. Phys. Lett.* **232** 407
[51] Stern T, Penhasi A and Cohen D 1995 *Biomaterials* **16** 17
[52] Flemming R G, Murphy C J, Abrams G A, Goodman S L and Nealey P F 1999 *Biomaterials* **20** 573
[53] Lin D T, Young T H and Fang Y 2001 *Biomaterials* **22** 1521
[54] Mori Y, Nagaoka S and Takiuchi H 1982 *Trans. Am. Soc. Artif. Organs.* **28** 459
[55] Ward R S, White K A and Hu C B 1984 *Polyurethanes in Biomedical Engineering* ed H Plank, G Egbers and I Syre (Amsterdam: Elsevier Science BV)
[56] Amitay-Sadovsky E, Ward B, Somorjai G A and Komvopoulos K 2003 *J. Phys. Chem.* B **107** 6377